

# Weierstraß–Institut für Angewandte Analysis und Stochastik

im Forschungsverbund Berlin e.V.

Preprint

ISSN 0946 – 8633

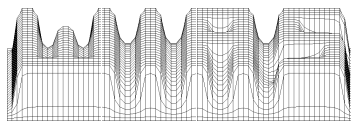
## Parameter estimation and geometrical optimal design for Bingham measurement devices

Dmitriy Logashenko<sup>1</sup>, Bernd Maar<sup>1</sup>, Volker Schulz<sup>2</sup>, Gabriel Wittum<sup>1</sup>

submitted: February 15th 2001

Preprint No. 642

Berlin 2001



*2000 Mathematics Subject Classification.* 65K05, 65N22, 76A05, 90C52.

*Key words and phrases.* Parameter estimation, optimal experimental design, Bingham fluids.

**Acknowledgement:** This research has been supported by the German federal ministry for research and education under grant number 03-WI7HE1-8.

---

<sup>1</sup>Interdisciplinary Center for Scientific Computing (IWR), University of Heidelberg, Im Neuenheimer Feld 368, 69120 Heidelberg, Germany

<sup>2</sup>Weierstrass Institute for Applied Analysis and Stochastics, Mohrenstrasse 39, D – 10117 Berlin, Germany, email: schulzv@wias-berlin.de

**Abstract.** Bingham models are frequently used for describing the flow of pastes. Usually, Bingham material parameters have to be determined in a rather cumbersome and time consuming manner. In this paper we develop a parameter estimation method for the automatic numerical determination of certain model parameters. The result is a tool for the simultaneous determination of all model parameters by using data from a single experiment sweep. Additionally, a method is presented to compute optimal shapes of corresponding measurement devices which lead to a high reliability of the resulting parameter estimation.

## 1 Introduction

Pastes are used, e.g. in the production of bricks from clay or bodies of catalytic converters from ceramic pastes. Usually they are extruded, where the quality of the extrusion product depends on the velocity distribution of the flow within the extrusion device. Recently, substantial progress has been achieved in the development of numerical simulation techniques for paste extrusion based on Bingham models [11]. However, in practice these numerical techniques can only be used, if certain parameters of the underlying flow model are known. These parameter values cannot be accessed by direct measurements, but are determined up to now in a process involving a rather high empirical effort and using analytical approximation approaches.

Therefore, we have developed parameter estimation techniques in a joint effort together with our industrial partner, Braun GmbH (Friedrichshafen), who already uses the numerical simulation techniques from [11] in the design of extrusion machines. Outlets for these extrusion machines are the main products of our industrial partner. The aim is the development of a model based measurement technique, which allows the simultaneous determination of all model parameters from one experiment and which is fast enough for online-usage. Since analytical approaches are not sufficient, a numerical parameter identification method is developed and implemented as software based on the *ug* toolbox [1].

However, as will be clarified later on, the statistical reliability of this approach is rather low for existing measurement devices. Therefore, methods of optimal experimental design are used to improve this reliability by geometry variations.

Optimal experimental design is a well known technique in many practical applications for linear system models. A good introduction can be found, e.g., in [13]. However, there are only few publications on optimal experimental design for nonlinear models and especially for models including differential equations. Most recent investigations are in the field of parameter identification and optimal control for ordinary differential equations and differential algebraic equations [9, 8, 5, 2]. In the second part of the paper we deal with an optimum experimental design problem in the form of a shape optimization problem for a highly nonlinear elliptic partial differential equations (PDE).

The paper is organized in the following way: In section 2 we describe the basic flow model used for the Bingham flow description. Section 3 explains the basic parameter identification formulation used in order to get values for the Bingham material parameters from measurements of normal flow stresses. In order to be able to solve the Bingham model equations, they have to be discretized, which is described in section 4. Based on the discretization and the parameter identification formulation, an algorithm for the solution of a resulting finite dimensional least-squares problem is given in section 5. This algorithm is based on inexact RSQP methods. Section 6 presents the basic definitions for the formulation of the optimal experimental design problems. In section 7 we investigate a specific experiment with real measurement data and show how necessary improvements to the current measurement technology are. Optimized devices are presented in section 8.

## 2 Bingham Fluids

The non-Newtonian flow of ceramic pastes can be described by the following PDE system from continuum mechanics for the case of incompressible fluids and low Mach number velocities (s. [6]): the continuity equation

$$\operatorname{div} \mathbf{u} = 0, \quad (2.1)$$

and the momentum equation

$$\rho \frac{\partial \mathbf{u}}{\partial t} = \operatorname{div} \mathbf{T} + \mathbf{f}, \quad (2.2)$$

where  $\rho$  is the (constant) density of the paste,  $\mathbf{u}$  is the velocity field of the flow,  $\mathbf{f}$  is a vector of the body forces and  $\mathbf{T}$  is the stress tensor. According to the angular momentum conservation law,  $\mathbf{T}$  is symmetric. It is usually assumed that it depends only on the pressure and the strain tensor

$$\mathbf{D} = \frac{1}{2} (\nabla \mathbf{u} + (\nabla \mathbf{u})^T).$$

In general form this dependence can be written as follows:

$$\mathbf{T} = -pI + \mathbf{T}^E(\mathbf{D}), \quad (2.3)$$

where  $p$  is the pressure and  $\mathbf{T}^E$  the extra stress tensor describing the viscous forces in the fluid. The special choice of the extra stress tensor specifies the mathematical model of the ceramic pastes.

For the materials we are interested in, the following form of the extra stress tensor is used (s. [10, 11]):

$$\mathbf{T}^E(\mathbf{D}) = 2\mu(\mathbf{D})\mathbf{D} = 2 \left( \eta_B + \tau_F (2\mathbb{I}_{\mathbf{D}})^{-\frac{1}{2}} \right) \mathbf{D}. \quad (2.4)$$

(Here  $\mathbb{I}_{\mathbf{D}}$  is the second invariant of  $\mathbf{D}$ ,  $\mathbb{I}_{\mathbf{D}} = \frac{1}{2}(\operatorname{Tr} \mathbf{D}^2 - (\operatorname{Tr} \mathbf{D})^2)$ .) But this form is assumed to be true if and only if

$$|\mathbb{I}_{\mathbf{T}^E}| > \tau_F^2. \quad (2.5)$$

Otherwise, i. e. if the inner stresses are small enough, the material is rigid and does not flow so that

$$\mathbf{D} = 0 \quad \text{for } |\mathbb{I}_{\mathbf{T}E}| \leq \tau_F^2. \quad (2.6)$$

Material whose flow is described by equations (2.1 – 2.2) with the stress tensor (2.3 – 2.4), under the condition (2.5), and (2.6) is called a *Bingham fluid*. The parameters  $\eta_B$  and  $\tau_F$  are said to be *Bingham viscosity* and *yield stress* respectively.

We shall consider only flow of ceramic pastes and assume that condition (2.5) is true respectively. Besides we shall consider only stationary flow, so that the time derivative in (2.2) is zero. The gravitation, being the only body force, does not play any essential role in our situation as well, because it is negligible in comparison with the viscous forces. Thus, further we omit also  $\mathbf{f}$ . This simplification leads to the following system describing our situation:

$$\begin{aligned} \operatorname{div} \mathbf{u} &= 0, \\ -\operatorname{div} (2\mu(\mathbf{D}) \cdot \mathbf{D}) + \nabla p &= 0. \end{aligned} \quad (2.7)$$

In this work, we consider only a two-dimensional model.

We would encounter difficulties when trying to get an approximate solution of system (2.7). The matter is that the extra stress tensor tends to infinity as the term  $\mathbb{I}_{\mathbf{D}}$  tends to zero. In reality this is not the case for the restriction (2.5) "switching" to the other equation, but omitting this condition we always come to such a situation. To avoid it, system (2.7) should be regularized. This means that we involve a small parameter  $\delta$  in the generalized viscosity function  $\mu$  so that

$$\mu(\mathbf{D}) = \eta_B + \tau_F(\delta + 2\mathbb{I}_{\mathbf{D}})^{-\frac{1}{2}}. \quad (2.8)$$

In this way we get an approximation of the system (2.7) at which  $\mu$  is bounded. The solution of the regularized system deviates from the unregularized Bingham solution. An exploration of the regularization error in a model problem is carried out in [11]. There, it is shown that this error tends to zero like  $O(\sqrt{\delta})$ .

**Remark:** As for incompressible fluids  $\operatorname{Tr} \mathbf{D} = 0$ ,  $\mathbb{I}_{\mathbf{D}} = \frac{1}{2}\operatorname{Tr} \mathbf{D}^2$ . Thus (2.8) attains the form

$$\mu(\mathbf{D}) = \eta_B + \tau_F(\delta + \operatorname{Tr} \mathbf{D}^2)^{-\frac{1}{2}}. \quad (2.9)$$

The stress tensor (2.3) attains the form

$$\mathbf{T} = -pI + 2\mu(\mathbf{D})\mathbf{D}. \quad (2.10)$$

In addition to these equations, the model of the ceramic pastes requires special boundary conditions. The reason for this is a phenomenon called wall sliding. Microscopically we have a two-phase flow on the boundary yielding a lubrication effect. Macroscopically this is described by sliding, resulting in a Navier-Type boundary condition that has in 2D the form

$$\begin{aligned} \mathbf{n}^T \mathbf{T} \mathbf{t} &= k\mathbf{u}^T \mathbf{t} + \tau_G, \\ \mathbf{u}^T \mathbf{n} &= 0. \end{aligned} \quad (2.11)$$

where  $\mathbf{t}$  and  $\mathbf{n}$  are the unit normal and unit tangent vectors to the boundary respectively. Here we assume that the tangential stress and the tangential velocity are

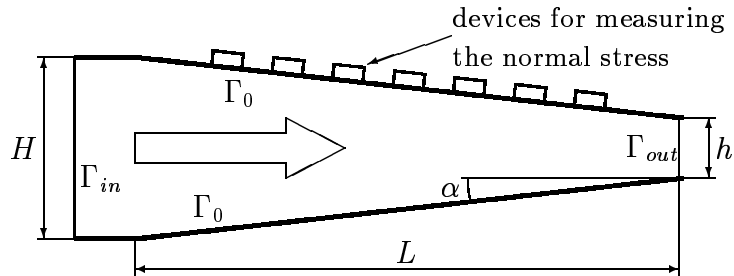


Figure 1: Scheme of the measurement device

codirected on the boundary. These condition include two additional scalar parameters: a wall sliding factor  $k$  and a sliding limit  $\tau_G$ .

Thus for the mathematical description of the flows of the ceramic pastes we have the system of PDEs (2.7) with the boundary conditions (2.11) on walls. (Besides inflow and outflow boundary conditions can be imposed on some parts of boundary). The whole model involves four parameters:  $\eta_B$ ,  $\tau_F$ ,  $k$  and  $\tau_G$ . The aim of the parameter estimation procedure described here is to find these values by using experimental data obtained by the device described in the next section. The nonlinearity of the PDE system together with its boundary conditions poses quite a challenge to the numerical treatment of the resulting parameter identification problem. It is necessary to note as well that the pressure  $p$  is defined by this system only up to a constant. Methods for the discretization of this system and numerical solution of the resulting nonlinear discrete equations are considered in detail in [11, 10].

### 3 Parameter Identification Technique

The parameters are estimated by using data obtained from a device whose scheme is shown on Fig. 1. This is a conical channel with rigid walls. The paste is pressed through this channel with constant velocity in the direction of the large arrow. During this process we measure the normal stress at seven fixed points on the upper wall (further referred to as *measurement points*). The values of the normal stress, as well as the inflow velocity of the paste, are then used for the parameter identification.

For the experiments we used the device with the following sizes:  $H = 30$  mm,  $h = 10$  mm,  $L = 244$  mm, so  $\alpha = 2.35^\circ$ . The inflow velocity was about  $80 \frac{mm}{s}$  (s. the experimental data below). Fig. 2 shows a photo of the device.

To model the flow of the paste inside the device we consider the interior (the polygon) as a region  $\Omega$  on which we impose the PDE system (2.7) with the generalized viscosity function (2.9). On the part  $\Gamma_0 \subset \partial\Omega$  of the boundary corresponding to the rigid walls we assume boundary conditions (2.11). On the inflow boundary  $\Gamma_{in}$  we impose Dirichlet boundary conditions for the velocity specifying the constant inflow velocity  $v_0$  along the whole segment. On the outflow boundary  $\Gamma_{out}$  we impose zero vertical

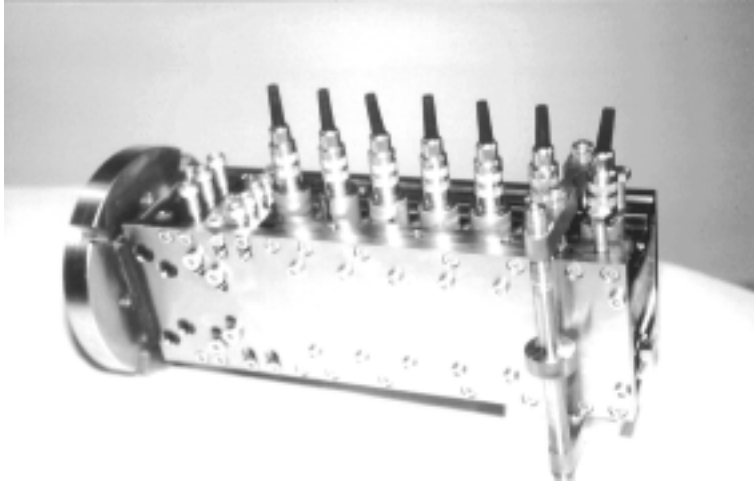


Figure 2: Photo of the measurement device

velocity as boundary condition and require  $\int_{\Gamma_{out}} p ds = \text{const.}$  For every set  $q = (\eta_B, \tau_F, k, \tau_G)^T$  of four parameters this system defines the velocity field  $\mathbf{u}$  and the pressure field  $p$ . Further we write all the partial differential equations comprising the system (2.7) and the boundary conditions in the form

$$\mathbf{c}(\mathbf{u}, p, q) = 0. \quad (3.1)$$

Denote the measurement points by  $P_1, P_2, \dots, P_K$  (in our case  $K = 7$ ), in the order from the outflow. For every  $P_i$  we have a measured value  $\hat{\pi}_i$  of the normal stress. In the same time, for every given set  $q$  of the parameters we can get the fields  $\mathbf{u}$  and  $p$  from equation (3.1) and compute the normal stress  $\pi_P(\mathbf{u}, p, q)$  at every point  $P \in \Gamma_0$ :

$$\pi_P(\mathbf{u}, p, q) = \mathbf{n}_P^T \mathbf{T}_P(\mathbf{u}, p, q) \mathbf{n}_P,$$

where  $\mathbf{n}_P$  and  $\mathbf{T}_P(\mathbf{u}, p, q)$  respectively are the unit normal vector to the boundary and the stress tensor (2.3) at the point  $P$ . The “correct” parameters are then determined as the solution of the nonlinear constrained optimization problem

$$\begin{aligned} f(\mathbf{u}, p, q) &= \sum_{i=2}^K \frac{1}{\sigma_i^2} \left( (\pi_{P_i}(\mathbf{u}, p, q) - \pi_{P_1}(\mathbf{u}, p, q)) - (\hat{\pi}_i - \hat{\pi}_1) \right)^2 \rightarrow \min \\ \text{s. t. } \mathbf{c}(\mathbf{u}, p, q) &= 0, \end{aligned} \quad (3.2)$$

where  $\sigma_i = 0.08(\hat{\pi}_i + \hat{\pi}_1)$  are the standard deviations for the difference evaluations, if all measurements are assumed to be independently normally distributed with expectation  $\hat{\pi}_i$  and standard deviation  $0.08\hat{\pi}_i$ . Although the model defines the normal stress only up to a constant, the differences of the stresses are defined exactly and should approximate the differences of the measured normal stresses. The numerical solution is carried out in a direct approach, i.e. by discretization of the model and the objective functional. This leads to a finite dimensional nonlinearly constrained optimization problem of a very large size that requires the application of structure exploiting methods to reduce the computation time.

## 4 Discretization of the Model

We discretize the PDE system (2.7) by the finite volume method from [11]. The application of this method to Bingham equations is similar to the case of a simple Stokes equation and inherits the similar problems. The implementation is based on *ug*-modules described for Navier-Stokes equations in [14].

We discretize the velocity and pressure fields on quadrilateral elements using a collocated scheme. Such discretizations require stabilization (cf. [3]). For the stabilization the idea described in [15] is used. This technique introduces a new term into the continuity equation, yielding:

$$-\gamma^2 \operatorname{div} \nabla p + \operatorname{div} \mathbf{u} = 0$$

with a scalar stabilization parameter  $\gamma$ . The influence of this stabilization term to the discretization of the Bingham model is discussed in [11]. The stabilization from [15] does not require any additional stabilization parameters.

Discretizing the outflow boundary conditions we use so called natural boundary conditions of our finite-volume scheme, namely  $\int_{\Gamma_{out}} p \, ds = \text{const}$ . That determines the pressure completely. The constant is given by the stabilization.

Further we shall denote the whole discretized system by

$$\mathbf{c}_h(\mathbf{u}, p, q) = 0. \tag{4.1}$$

Here  $\mathbf{u}$  and  $p$  are respectively two- and one-dimensional grid functions defined on the same index sets. We underline that this is a nonlinear system for all variables. Further it will be also convenient to denote a set  $(\mathbf{u}, p)$  by the single letter  $\mathbf{x}$ . So we shall write  $\mathbf{c}_h(\mathbf{x}, q)$  instead of  $\mathbf{c}_h(\mathbf{u}, p, q)$ .

Since we aim at fast solution techniques we employ multigrid methods for the solution of (4.1). However, the direct application of multigrid methods (with an ILU smoother) to the linearized system from a Newton approach fails. Therefore we rewrite the discretized system (4.1) in the form

$$\mathbf{A}(\mathbf{x}, q) \mathbf{x} = \mathbf{f}, \tag{4.2}$$

where  $\mathbf{A}$  is a sparse matrix. Based on this form we can easily apply a fixed-point method with inner linear multi-grid solvers.

The grid levels were obtained by uniform refinement of a coarser grid containing less than hundred quadrilaterals. The matrices on each grid level were constructed by discretization of the PDE system. In Fig. 3 we show an example of numerical results obtained by this discretization.

For the discretization of the whole system the strain tensor  $\mathbf{D}$  and the generalized viscosity function were also defined using finite dimensional grid functions  $\mathbf{u}$ . This allows to discretize the normal stress functions  $\pi_{P_i}$ . We denote the discrete variants by  $\pi_{h,i}$  respectively. This completes the discretization of the whole optimization

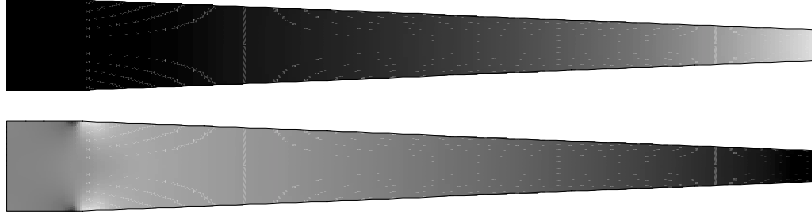


Figure 3: Results of the numerical simulation of a flow in the measurement device. The upper picture shows the horizontal velocity, the lower one — the pressure

problem which now reads

$$f_h(\mathbf{x}, q) = \sum_{i=2}^K \frac{1}{\sigma_i^2} \left( (\pi_{h,i}(\mathbf{x}, q) - \pi_{h,1}(\mathbf{x}, q)) - (\hat{\pi}_i - \hat{\pi}_1) \right)^2 \rightarrow \min \quad (4.3)$$

s. t.  $\mathbf{c}_h(\mathbf{x}, q) = 0$ .

This is a nonlinearly constrained finite dimensional optimization problem.

## 5 The Parameter Estimation Procedure

Here we consider the optimization problem (4.3) in the abstract form, omitting the subscript  $h$ :

$$f(\mathbf{x}, q) \rightarrow \min, \quad (5.1)$$

s. t.  $\mathbf{c}(\mathbf{x}, q) = 0$ ,

with  $f : \mathbf{R}^{n \times m} \rightarrow \mathbf{R}$  and  $c : \mathbf{R}^{n \times m} \rightarrow \mathbf{R}^n$  and the Jacobian,  $\mathbf{J} = \frac{\partial \mathbf{c}}{\partial \mathbf{x}}$ , which is assumed to be nonsingular. In our case the number of parameters is 4. However,  $n$ , the dimension of the grid functions, can be very large.

For the solution of the problem (5.1) we use a reduced SQP method. A detailed discussion of this approach can be found in [16, 17]. Here we sketch only the idea.

Reduced SQP methods are related to projected Lagrangian methods (cf. [4]) and are most advantageous in the case that the number of degrees of freedom (here the parameters) is small compared to the number of state variables. The constraints are linearized by a Taylor expansion up to first order terms, so that all steps  $(\Delta \mathbf{x}, \Delta q)$  lie in the tangent space of  $\mathbf{c}$  of the current approximation  $(\mathbf{x}, q)$ :

$$\mathbf{c}(\mathbf{x}, q) + \mathbf{J}(\mathbf{x}, q) \Delta \mathbf{x} + \frac{\partial \mathbf{c}}{\partial q}(\mathbf{x}, q) \Delta q = 0.$$

Then the problem is projected to this tangent space and approximated by a quadratic problem with the projected Hessian of the Lagrangian

$$L(\mathbf{x}, q, \lambda) = f(\mathbf{x}, q) - \lambda^T \mathbf{c}(\mathbf{x}, q). \quad (5.2)$$

In this formulation the algorithm reads:

**Algorithm 1:** The RSQP method.

- (0) Set  $k := 0$ ; start at some initial guess  $\mathbf{x}_0, q_0$ .
- (1) Compute the adjoint variables from the linear system  $\mathbf{J}^T(\mathbf{x}_k, q_k) \lambda_{k+1} := \nabla_{\mathbf{x}} f(\mathbf{x}_k, q_k)$ ;  
compute the reduced gradient  $\gamma_k := \nabla_q f(\mathbf{x}_k, q_k) - \left( \frac{\partial \mathbf{c}}{\partial q}(\mathbf{x}_k, q_k) \right)^T \lambda_{k+1}$ ;  
determine some approximation  $B_k$  of the projected Hessian of the Lagrangian.
- (2) solve  $B_k \Delta q_k = -\gamma_k$ .
- (3) compute step on  $\mathbf{x}$  from the linear system  $\mathbf{J}(\mathbf{x}_k, q_k) \Delta \mathbf{x}_k := -\frac{\partial \mathbf{c}}{\partial q}(\mathbf{x}_k, q_k) \Delta q_k + \mathbf{c}(\mathbf{x}_k, q_k)$ .
- (4) Set  $\mathbf{x}_{k+1} := \mathbf{x}_k + \Delta \mathbf{x}_k, q_{k+1} := q_k + \Delta q_k$ .
- (5)  $k := k + 1$ ; go to (1) until convergence.

The computationally expensive operation of evaluation of the projected Hessian is avoided by using update formulas: at the first iteration some initial approximation, for example

$$B_0 = \alpha I \tag{5.3}$$

with a positive scalar  $\alpha$ , is taken. Then every next approximation is computed from the previous one by a formula

$$B_{k+1} = B_k + \text{Update}(B_k, s_k, v_k). \tag{5.4}$$

There exist different update strategies (s. [4, 16]), for instance the BFGS update formula reads:

$$\text{Update}(B, s, v) = \frac{vv^T}{v^T s} - \frac{(Bs)(Bs)^T}{s^T Bs}. \tag{5.5}$$

For the arguments of this update one can take vectors

$$s_k := q_k - q_{k-1}, \quad v_k := \gamma_k - \gamma_{k-1}. \tag{5.6}$$

It can be proven that under mild conditions the reduced SQP method described by Algorithm 1 with the BFGS update formula (5.4 – 5.6) shows 2-step superlinear local convergence (s. [16]).

In the Algorithm 1, it is necessary to invert the Jacobian  $\mathbf{J}$  of the constraints. As we mentioned in the previous section, this approach is not recommendable. The following consideration allows to replace  $\mathbf{J}$  with the fixed point iteration matrix  $\mathbf{A}$ .

To this end we incorporate the reduced SQP algorithm within the previously mentioned fixed point iteration instead of a Newton iteration—in the spirit of inexact reduced SQP methods as considered in [17]. Carrying out the fixed point iteration instead one obtains an algorithm that does not involve inversion of  $\mathbf{J}$  or  $\mathbf{J}^T$ . Nevertheless the Jacobian is still used for computation of the correct adjoint variables and the correct state increments in the sense of defect correcting iterations:

**Algorithm 2:** The RSQP method with an approximate Jacobian.

- (0) Set  $k := 0$ ; start at some initial guess  $\mathbf{x}_0, q_0$ .
- (1) Compute the increment of the adjoint variables from the linear system  $\mathbf{A}^T(\mathbf{x}_k, q_k) \Delta \lambda_k := \nabla_{\mathbf{x}} f(\mathbf{x}_k, q_k) - \mathbf{J}^T(\mathbf{x}_k, q_k) \lambda_k$ ;  
compute the reduced gradient  $\gamma_k := \nabla_q f(\mathbf{x}_k, q_k) - \left( \frac{\partial \mathbf{c}}{\partial q}(\mathbf{x}_k, q_k) \right)^T (\lambda_k + \Delta \lambda_k)$ ;  
determine some approximation  $B_k$  of the projected Hessian of the Lagrangian.
- (2) solve  $B_k \Delta q_k = -\gamma_k$ .
- (3) compute step on  $\mathbf{x}$  form the linear system  $\mathbf{A}(\mathbf{x}_k, q_k) \Delta \mathbf{x}_k := -\frac{\partial \mathbf{c}}{\partial q}(\mathbf{x}_k, q_k) \Delta q_k + \mathbf{c}(\mathbf{x}_k, q_k)$ .
- (4) Set  $\mathbf{x}_{k+1} := \mathbf{x}_k + \Delta \mathbf{x}_k, q_{k+1} := q_k + \Delta q_k$  and  $\lambda_{k+1} = \lambda_k + \Delta \lambda_k$ .
- (5)  $k := k + 1$ ; go to (1) until convergence.

A step of this method can be also interpreted as an approximate Newton step for the necessary conditions of extremum for the problem (5.1) since the updates of the variables are computed according to a linear system

$$\begin{pmatrix} 0 & 0 & \mathbf{A}^T \\ 0 & B_k & \left( \frac{\partial \mathbf{c}}{\partial q} \right)^T \\ \mathbf{A} & \frac{\partial \mathbf{c}}{\partial q} & 0 \end{pmatrix} \begin{pmatrix} \Delta \mathbf{x} \\ \Delta q \\ \Delta \lambda \end{pmatrix} = \begin{pmatrix} \nabla_{\mathbf{x}} L \\ \nabla_q L \\ -\mathbf{c} \end{pmatrix}. \quad (5.7)$$

Some notes on the convergence properties of the reduced SQP methods can be found in [17]. The positive definiteness of the approximations  $B_k$  should be preserved. The BGFS update formula (5.4 – 5.5) yields a positive definite  $B_{k+1}$  for a positive definite  $B_k$  if and only if  $v_k^T s_k > 0$  (s. [4]). In the RSQP method started with an arbitrary initial guess this property can be violated that can lead to indefinite approximations of the Hessian. As a remedy we used the Powell modification of the BGFS update formula [12].

The next important issue is that these methods converge only locally and starting with an arbitrary initial approximation Algorithm 2 always requires some damping in step 4. The damping factor is usually chosen by a line search. It is required that the damping parameter supplies sufficient descent of a merit function that involves the constraint as well as the value of the objective function. This is done to provide also the approximate feasibility of the guess. We used the merit function

$$\psi(\mathbf{x}, q) = f(\mathbf{x}, q) + \sum_i \mu_i |c_i(\mathbf{x}, q)|, \quad (5.8)$$

where  $\mu_i > 0$  are estimated upper bounds for the absolute values of the adjoint variables ( $|\lambda_i|$ ) at the optimal solution. This merit function supplied good convergence properties up to practical precision.

For the computations we implemented Algorithm 2 with the Powell modification of the BGFS update formula. The initial approximation to the Hessian was  $B_0 = I$ . For the initial guess of the parameters we took some reasonable values. As the

initial guess for  $\mathbf{x}$  we took an approximate solution of the constraint for the initial parameters obtained by the fixed point iteration. For the solution of the large sparse linear systems with the matrices  $\mathbf{A}$  and  $\mathbf{A}^T$  we applied the above mentioned multigrid method with *ILLU* smoothing. This provided an approximate feasibility in the first iteration. The initial values of the adjoint variables were merely  $\lambda_0 = 0$ .

## 6 Confidence Intervals of the Computed Parameters

We estimate the precision of the represented measurement technique by computing the confidence intervals for the obtained parameters according to the linearized model. To this end we assume that the errors of the measurements at the measurement points are statistically independent and meet the normal distribution. Let  $\Pi : \mathbf{R}^n \times \mathbf{R}^4 \rightarrow \mathbf{R}^6$  be a function that assigns the theoretical relative normal stresses to a given guess  $\mathbf{x}$  and a given set of parameters:

$$\Pi(\mathbf{x}, q) = (\pi_2(\mathbf{x}, q) - \pi_1(\mathbf{x}, q), \dots, \pi_7(\mathbf{x}, q) - \pi_1(\mathbf{x}, q))^T.$$

As the velocity and pressure fields corresponding to the parameters  $q$  satisfy the equation  $\mathbf{c}(\mathbf{x}, q) = 0$ , the full differential of the function assigning the normal stresses at the measurement points to the parameters is a matrix

$$S(q) = \begin{pmatrix} \frac{\partial \Pi}{\partial \mathbf{x}} & \frac{\partial \Pi}{\partial q} \end{pmatrix} \begin{pmatrix} -J^{-1} \frac{\partial c}{\partial q} \\ I \end{pmatrix}$$

(all the functions should be evaluated at  $(\mathbf{x}, q)$ , with  $\mathbf{c}(\mathbf{x}, q) = 0$ ). Now the covariances corresponding to the parameters  $q$  are the diagonal entries of the matrix

$$\begin{aligned} \mathbf{Cov}(q) &= \left[ (S(q))^T D^{-2} S(q) \right]^{-1} \\ &= \left[ \begin{pmatrix} -J^{-1} \frac{\partial c}{\partial q} \\ I \end{pmatrix}^T \begin{pmatrix} \left( \frac{\partial \Pi}{\partial \mathbf{x}} \right)^T \\ \left( \frac{\partial \Pi}{\partial q} \right)^T \end{pmatrix} D^{-2} \begin{pmatrix} \frac{\partial \Pi}{\partial \mathbf{x}} & \frac{\partial \Pi}{\partial q} \end{pmatrix} \begin{pmatrix} -J^{-1} \frac{\partial c}{\partial q} \\ I \end{pmatrix} \right]^{-1}, \end{aligned} \quad (6.1)$$

where  $D = \text{diag} \{0.08(\hat{\pi}_{i-1} + \hat{\pi}_1)\}$  for the precision of the measurements 8%. Then for every parameter  $p$  ( $p$  can be  $\eta_B$ ,  $\tau_F$ ,  $k$  or  $\tau_G$ ) the 95%-confidence interval is  $p \pm 3.182\sqrt{(\mathbf{Cov}(q))_{pp}}$ .

As we shall see, the confidence intervals of the parameters measured using the simple device shown on Fig. 1 are too large and unacceptable for industrial purposes. This disadvantage can be corrected by the shape optimization of the device.

## 7 Experiment

Here we show results of one of the experiments. For this experiment we used the device with the following sizes:  $H = 30 \text{ mm}$ ,  $h = 10 \text{ mm}$ ,  $L = 244 \text{ mm}$ ,  $\alpha \approx 2.35^\circ$

Measurement point	$P_1$	$P_2$	$P_3$	$P_4$	$P_5$	$P_6$	$P_7$
Normal stresses (bar)	2.66	5.2	7.45	9.3	11.2	12.4	13.5

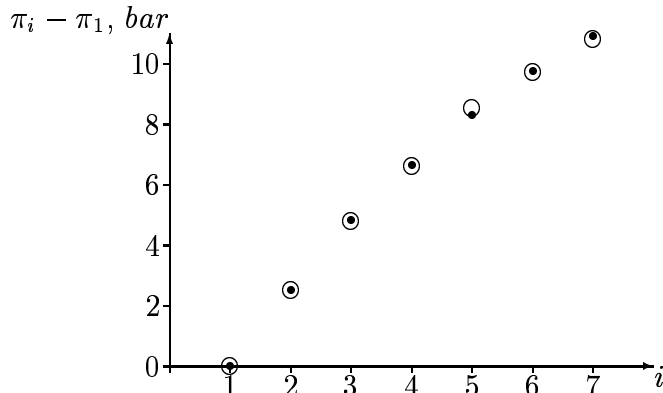


Figure 4: The differences of the normal stresses. Empty circles denote the relative measured stresses ( $\hat{\pi}_i - \hat{\pi}_1$ ), and the black circles show the stresses  $\pi_{h,i}(\mathbf{x}, q) - \pi_{h,1}(\mathbf{x}, q)$  computed for the final guess  $(\mathbf{x}, q)$  of the optimization procedure. The difference  $\pi_{h,1}(\mathbf{x}, q) - \hat{\pi}_1$  is 13.75

(s. Fig. 1). The paste was pressed through the device at the average inflow velocity  $v_0 = 80 \frac{mm}{s}$ . The measured normal stresses on the upper wall are listed in Table 1. The measurement points are numbered here from the outlet. The precision of the measurements is  $\pm 8\%$ .

Because of the comparatively low measurement precision the normal stresses obtained from the model do not coincide with the measured ones. The measured stresses do not correspond to real material parameters, so the minimum value of the objective function that can be expected is not equal to 0.

The optimization procedure was started with the initial parameters

$$\eta_B = 0.0005 \text{ bar} \cdot s, \quad \tau_F = 3 \text{ bar}, \quad k = 0.5 \frac{\text{bar} \cdot s}{m}, \quad \tau_G = 0.15 \text{ bar}$$

on a grid with 969 nodes (896 quadrilaterals) on the finest level. For the regularization constant  $\delta$  we have chosen a value 0.01. The computed stresses after the parameter estimation are compared with the measurements in Fig. 4.

Table 3 represents also the 95% confidence intervals computed for the standard deviation of 0.05 bar of the measured normal stresses. Computation of the covariance matrix requires inverting the Jacobian  $J$  that proved to be a very ill conditioned matrix.

As one can see the precision of the method is very poor for all parameters. This happens because in this device, the dependence of the simulated relative normal stresses at the measurement points on the parameters is very weak. This fact can be easily seen from numerical experiments: quite different sets of the parameters

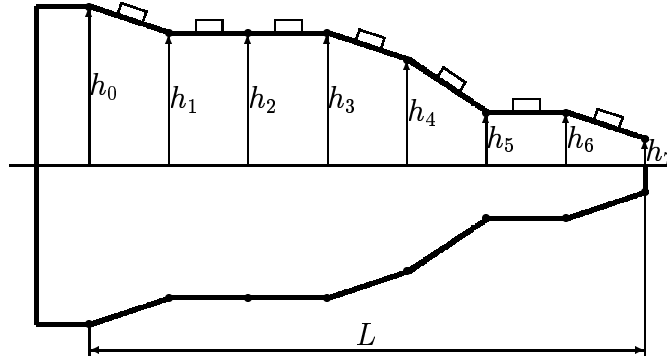


Figure 5: Scheme of the measurement device shape at the shape optimization

yield quite similar differences of the normal stresses. As a remedy one can propose to change the shape of the device. We discuss this question in the next section.

## 8 Optimization of the shape of the device

One can try to improve the confidence intervals by varying the shape of the device. We consider measurement devices with piecewise planar boundaries (Fig. 5). There are 7 pieces and the measurement points are located at the centers of the segments. The horizontal projections of the pieces always have equal length, but the heights  $h_i$  are varied. We look for a device that for a given set  $q$  of parameters, provides the smallest (in some sense) confidence intervals for all the parameters. As the criterion for the minimization we choose the value

$$\Phi(\mathbf{Cov}) = \frac{1}{4} \text{Tr } \mathbf{Cov}$$

(A-optimal design).

Here we need the following assumption. As the model determines the normal stresses up to a constant only, the real absolute values of these stresses are unknown, and it is impossible to determine absolute values of relative errors. So we assume that the measurements at all the measurement points are carried out with the same standard deviation  $\sigma = 0.05 \text{ bar}$ . Then we can compute the relative covariations according the formula (6.1) with  $D = 2I$  (because the standard deviation of the differences is then  $2\sigma$ ), the confidence intervals being  $\pm 3.182\sigma \sqrt{(\mathbf{Cov}(q))_{pp}}$

We also impose some restriction on the shape of the device. First, it is reasonable to consider only devices with  $h_0 \geq h_1 \geq \dots \geq h_7$ . Then, the practice shows that the heights  $h_i$  should be restricted above and below to avoid extremally large or small values. So the complete optimization problem is: for a given set  $q$  of the parameters, find  $h_0, \dots, h_7$  such that

$$\begin{aligned} \Phi(\mathbf{Cov}(q)) &= \frac{1}{4} \text{Tr } \mathbf{Cov}(q) \rightarrow \min \\ \text{s. t. } & h_0 \geq \dots \geq h_7, \\ & h_0 \geq h_{\min}, \quad h_7 \leq h_{\max}. \end{aligned}$$

Note that the objective functional of this problem requires computation of  $\mathbf{x}$  such that  $c(\mathbf{x}, q) = 0$ , i. e. simulation of the flow of the paste in the device. As the variables  $h_i$  are included in the problem implicitly (they determine the shape of the domain), it is hardly possible to differentiate the objective functional with respect to them. This implies application of a numerical optimization procedure that does not use the gradients. We applied a direct search method for nonlinear optimization [7], which resulted in  $h_i$ -values as listed in Table 2.

Table 2: The values of  $h_i$  for the optimized device.

$i$	0	1	2	3	4	5	6	7
$h_i, mm$	59.7	31.8	31.8	25.8	22.7	4.9	3.0	3.0

At the computations, the length of the device was assumed to be  $L = 240 mm$ . The optimization procedure was started with a simple quadrilateral shape (like that on the Fig. 1) of the followigh size:  $h_0 = 30 mm$ ,  $h_7 = 6 mm$ . The inflow velocity was  $80 \frac{mm}{s}$  as before. The optimization was carried out for the parameter set from Table 2. For the maximal possible value of the height  $h_i$  we have chosen the doubled initial value of  $h_0$ , i. e.  $h_{\max} = 60 mm$ . Analogously, the minimal possible value was  $h_{\min} = 3 mm$  — the halved initial value of  $h_7$ .



Figure 6: Simulation of flows in the optimized device (7 segments). The upper picture shows the horizontal velocity, the lower one — the pressure.

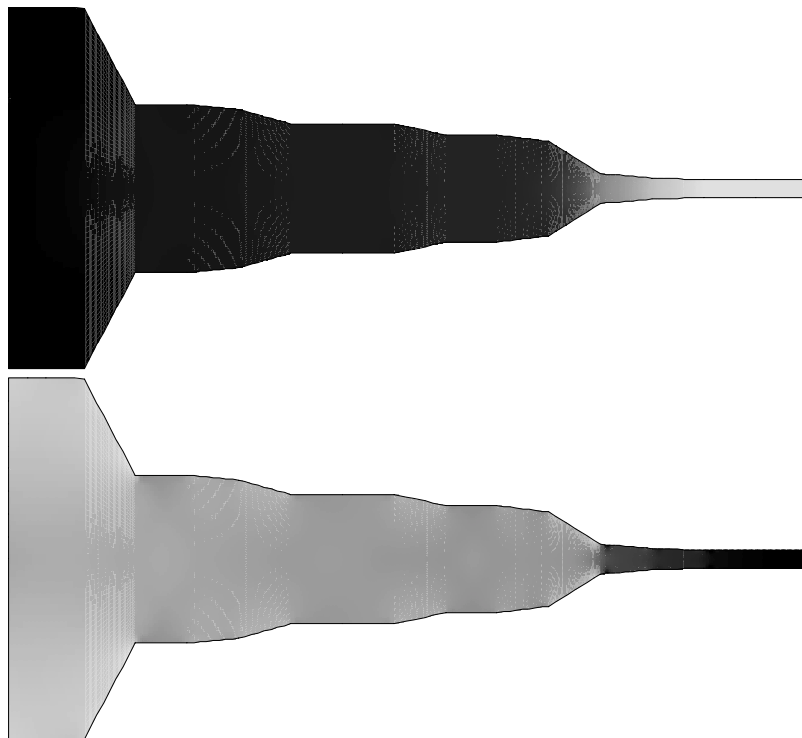


Figure 7: Simulation of flows in the optimized device (15 segments). The upper picture shows the horizontal velocity, the lower one — the pressure.

The shape of the device after the optimization is described by the heights  $h_i$  in the Table 2. Results of a simulation of the flows in this device are shown on Fig. 6. Table 3 shows the relative covariances and the confidence intervals for the optimized case in comparison with those for the simple shape described in the previous chapters.

The geometry of the measurement device is described here as a piecewise linear function with a predefined sequence of heights. This can be considered an approximation of the “true” optimal solution taken from an infinite function space. Of course, the existence of such a function space solution cannot be guaranteed theoretically for this highly complex shape optimization problem. In order to reassure our solution somewhat in this sense we recompute the shape optimization with 15 segments instead of the 7 segments before. The resulting Fig. 7 is very similar to Fig. 6, and also the resulting confidence intervals are almost identical, thus providing more confidence in our optimal shape.

## 9 Conclusions

In this project, we have developed a parameter estimation technique based on measuring the stresses in a flow, and comparing them with the simulated ones. As it was shown, this method works only with the special construction of the measurement device, else it demonstrates a very poor precision. This construction was obtained by means of the shape optimization.

Table 3: The parameters and the confidence intervals

Parameter	The simple shape		The optimized shape	
	Rel. covariance	Conf. interval	Rel. covariance	Conf. interval
$\eta_B = 0.302 \text{ bar} \cdot \text{s}$	27298.8	$\pm 26.287$	$9.13 \cdot 10^{-4}$	$\pm 0.0048$
$\tau_F = 3.03 \text{ bar}$	58651.2	$\pm 38.531$	0.107	$\pm 0.052$
$k = 0.497 \frac{\text{bar} \cdot \text{s}}{\text{m}}$	84305.5	$\pm 46.195$	0.188	$\pm 0.069$
$\tau_G = 0.180 \text{ bar}$	86.3207	$\pm 1.478$	0.259	$\pm 0.081$

## References

- [1] P. Bastian, K. Birken, K. Johannsen, S. Lang, N. Neuß, H. Rentz-Reichert, and C. Wieners. UG – a flexible software toolbox for solving partial differential equations. *Computing and Visualization in Science*, 1:27–40, 1997.
- [2] I. Bauer, H.-G. Bock, S. Körkel, and J. Schlöder. Numerical methods for optimum experimental design in dae systems. in [18], 2000.
- [3] F. Brezzi and M. Fortin. *Mixed and Hybrid Finite Element Methods*. Springer, 1991.
- [4] P.E. Gill, W. Murray, and M.H. Wright. *Practical optimization*. Academic Press, London, 1981.
- [5] K.-D. Hilf. *Optimale Versuchsplanung zur dynamischen Roboterkalibrierung*, volume 8 of *Fortschrittsberichte*. VDI-Verlag, Düsseldorf, 1996.
- [6] L. Landau and E. Lifschitz. *Lehrbuch der Theoretischen Physik. Band VI, Hydrodynamik*. Akademischer Verlag, Berlin, 1991.
- [7] R. Lewis, V. Torczon, and M. Trosset. Direct search methods: then and now. *J. Comput. Appl. Math.*, 124(1-2):191–207, 2000.
- [8] T. Lohmann. *Ein numerisches Verfahren zur Berechnung optimaler Versuchspläne für beschränkte Parameteridentifizierungsprobleme*. Reihe Informatik. Shaker, Aachen, 1993.
- [9] Th. Lohmann, H.-G., and J. Schlöder. Numerical methods for parameter identification and optimal experimental design in chemical reaction systems. *Ind. Eng. Chem. Res.*, 31:54–57, 1992.
- [10] C. Lund. *Ein Verfahren zur numerischen Simulation instationärer Strömungen mit nichtlinear-viskosen Fließeigenschaften*. Number 344 in Fortschr.-Ber. VDI Reihe 7. VDI Verlag, Düsseldorf, 1998.
- [11] B. Maar. *Nicht-Newtonische Fluide. Mehrgitterverfahren für Bingham-Strömungen*. PhD thesis, University of Stuttgart, 1998.
- [12] M.J.D. Powell. A fast algorithm for nonlinearly constrained optimization calculations. In G.A. Watson, editor, *Numerical Analysis Proceedings Dundee 1977*, pages 144–157. Springer-Verlag, 1978.

- [13] F. Pukelsheim. *Optimal design of experiments*. Wiley Series in Probability and Mathematical Statistics. Wiley, New York, 1993.
- [14] H. Renz-Reichert. *Robuste Mehrgitterverfahren zur Lösung der inkompressiblen Navier-Stokes Gleichung: Ein Vergleich*. PhD thesis, University of Stuttgart, 1996.
- [15] G. Schneider and M. Raw. Control volume finite-element method for heat transfer and fluid flow using collocated variables — 1. computational procedure. *Numerical Heat Transfer*, 11:363–390, 1987.
- [16] V.H. Schulz. *Reduced SQP methods for large-scale optimal control problems in DAE with application to path planning problems for satellite mounted robots*. PhD thesis, University of Heidelberg, 1996.
- [17] V.H. Schulz. Solving discretized optimization problems by partially reduced SQP methods. *Computing and Visualization in Science*, 1(2):83–96, 1998.
- [18] V.H. Schulz (guest-editor). Special issue on SQP-based direct discretization methods for practical optimal control problems. *Journal of Computational and Applied Mathematics*, 120(1-2), 2000.